### Data-driven Modeling and Predictive Control of Maximum Pressure Rise Rate in RCCI Engines

L. N. Aditya Basina<sup>1</sup>, Behrouz K. Irdmousa<sup>1</sup>, Javad Mohammadpour Velni<sup>2</sup>, Hoseinali Borhan<sup>3</sup>, Jeffrey D. Naber<sup>1</sup>, and Mahdi Shahbakhti<sup>4</sup>

Abstract—Reactivity controlled compression ignition (RCCI) is a promising low temperature combustion (LTC) regime that offers lower nitrogen oxides (NOx), soot and particulate matter (PM) emissions along with higher combustion efficiency compared to conventional diesel engines. It is critical to control maximum pressure rise rate (MPRR) in RCCI engines in order to safely and efficiently operate at varying engine loads. In this paper, a data-driven modeling (DDM) approach using support vector machines (SVM) is adapted to develop a linear parameter-varying (LPV) representation of MPRR for RCCI combustion. This LPV representation is then used in the design of a model predictive controller (MPC) to control crank angle of 50% of fuel mass fraction burn (CA50) and indicated mean effective pressure (IMEP) while limiting the MPRR. The results show that the LPV-MPC control strategy can track CA50 and IMEP with mean tracking errors of 0.9 CAD and 4.7 kPa, respectively, while limiting the MPRR to the maximum allowable value of 5.8 bar/CAD.

#### I. INTRODUCTION

RCCI combustion is an LTC regime that uses a blend of two fuels with different reactivity levels to control the combustion inside the combustion chamber. The low reactivity fuel is injected via the port fuel injectors (PFI) while the high reactivity fuel is injected via the direct injectors (DI) which forms reactivity gradient inside the combustion chamber. Ignition in RCCI occurs at high reactive regions and expands to low reactive regions inside the combustion chamber. This form of combustion initiation makes it difficult to control RCCI combustion and reach its low emission and high thermal efficiency benefits while avoiding its drawbacks including high carbon monoxide (CO) and unburned hydrocarbon emissions and high cyclic variability  $(COV_{IMEP})$  at certain operating regions [1]. Moreover, it is known that RCCI operation is difficult at high loads due to premixed form of RCCI combustion which results in auto-ignition at multiple regions inside combustion chamber and consequently high heat release rates. This limits RCCI operation at higher loads and results in high combustion

\*This work was supported by the United States National Science Foundation.

noise which is linked with high maximum pressure rise rate (MPRR) and is characterized by high ringing intensity (RI). Allowable MPRR in RCCI engines changes from one engine to another and depends on engine applications (e.g., heavy duty vs light duty applications). It is necessary to control engine load (IMEP) and MPRR to allow RCCI operation at varying engine load conditions.

Researchers have conducted studies to devise strategies to expand high load limitations in RCCI engines by finding effective parameters to reduce MPRR. Zoldak et. al [2] performed a computational fluid dynamics (CFD) study and concluded that in-cylinder reactivity gradient is enough to reduce MPRR in RCCI engines. However, high reactivity gradient may cause incomplete combustion [3]. In another study by Hanson et. al [4], it was found that MPRR in RCCI engines is dependent on temperature and pressure at intake valve closing (IVC), port fuel injected fuel mass, direct injected fuel mass, exhaust gas re-circulation (EGR) rate and in-cylinder temperature.

Zoldak et. al [2] studied the effects of double fuel injection strategy on MPRR thoroughly. Their research showed that retarding second injection reduces MPRR in RCCI engines. These studies provided strategies to control MPRR in RCCI engines which would help to expand high load operation in RCCI engines. However, all these studies were conducted under steady state engine operations. The developed MPRR controllers for RCCI engines only control MPRR passively by avoiding high MPRR regions of operation. MPRR in RCCI engines can be actively controlled by implementing a closed-loop control strategy. There are limited studies on closed-loop control of RCCI engines in literature. The prior studies can broadly be split into two categories, simulation studies and experimental studies. Simulation studies used validated RCCI engine model to verify designed RCCI controller performance while experimental studies implemented the developed RCCI controller on a real RCCI engine.

A study was undertaken by Kannan [5] and later by Arora et al. [6] to understand the effect of different control knobs on the combustion of an RCCI engine and to develop a PI controller to adjust CA50 and IMEP and to enable mode switching between RCCI and SI combustion. The implementation showed that there is a high cyclic variability which has to be addressed for smooth operation and consistent control. Kondipati et al. [7] further explored different control knobs for the control of CA50. A sensitivity map was generated for CA50 versus start of injection (SOI) and Premixed Ratio

 $<sup>^1</sup>$ L. N. Aditya Basina, Behrouz K Irdmousa and Jeffrey D. Naber are with the Mechanical Engineering-Engineering Mechanics Department at Michigan Technological University, {abasina, bkhoshi, jnaber } @mtu.edu

 $<sup>^2</sup>$ Javad Mohammadpour Velni is with the School of Electrical and Computer Engineering, University of Georgia, javadm @uga.edu

<sup>&</sup>lt;sup>3</sup>Hoseinali Borhan is with Cummins Inc, hoseinali.borhan @cummins.com

<sup>&</sup>lt;sup>4</sup>Mahdi Shahbakhti is with the Department of Mechanical Engineering, University of Alberta, mahdi @ualberta.ca

(PR). This map was proposed for selecting SOI or PR to control CA50 depending on the operating condition. Some model-based controllers have been developed in the recent years for RCCI engines. Sadabadi et al. [8] created a controloriented model (COM) based on physical modeling which was validated with an experimentally verified CFD model. This COM was used as the plant model for an RCCI engine to build a linear quadratic regulator (LQR) to control CA50 with PR. This COM was later augmented with a model for fuel transport during transient operations developed by Raut et al. [10] based on the work of Shahbkahti et al. [9]. The augmented COM was then used to develop an MPC to control CA50 and IMEP and was validated experimentally on an RCCI engine. Feedforward values from experimental data were used to keep the  $COV_{IMEP}$  below 5% and limit cyclic variability.

Numerical analysis has been also used to develop linearized models for RCCI control. Indrajauna et al. [11] created a multi-zone combustion model that was capable of predicting the pressure trace. This model was then experimentally validated and used for developing a linearized model for controlling ignition delay and IMEP. However, the implemented controllers only control CA50 and IMEP but not pressure rise rate.

The development of physics based combustion controller takes considerable amount of time and effort. An alternative approach is to utilize DDM to develop RCCI models. In particular, DDM methods that can generate dynamic statespace models that can be used for controller design are of interest. Khoshbakht Irdmousa et al. [12] presented a support vector machine (SVM) based DDM approach to develop an LPV state space representation of an RCCI engine that was used by an MPC to control combustion phasing of an RCCI engine. Building on our prior work [12] this work generates an LPV representation of an RCCI engine that predicts the MPRR and uses it to develop an MPC to actively limit the MPRR in RCCI engines.

To the best of author's knowledge, this paper presents the first study undertaken to develop a model-based RCCI controller to adjust MPRR, while controlling IMEP and CA50. The contributions of this work are two folds. First, it creates the first data-driven LPV model for predicting MPRR in RCCI engines. Second, it designs a new closed-loop control framework that controls cycle-by-cycle MPRR, IMEP and CA50 for RCCI engine transient operations.

This paper is organized as follows. The dynamic RCCI model is explained in Section II. Next, generation of LPV state-space model is discussed in Section III. At Section IV, development of model predictive controller and results will be presented. Finally, summary of obtained knowledge from this research is presented in Section V.

## II. CYCLE BY CYCLE PHYSICS BASED DYNAMIC RCCI ENGINE MODEL

This work uses a cycle by cycle RCCI engine model from our prior work [13] which was validated at a wide range of steady-state and transient conditions against experimental data. The model is capable of predicting CA50, IMEP, MPRR,  $P_{soc}$ ,  $T_{soc}$  along with other parameters of interest at every engine cycle. The model is parametrized for a 2-liter RCCI engine. Details about engine and experimental setup are found in reference [10].

A sample transient validation of the RCCI dynamic model for predicting cycle by cycle MPRR is shown in Fig. 1. The results in Fig. 1 show that the RCCI model predicts MPRR with an average error of 0.6 bar/CAD. The data from this experimentally validated RCCI model is used in this study to illustrate the development of an SVM based data-driven model for predicting and control of MPRR in RCCI engines.

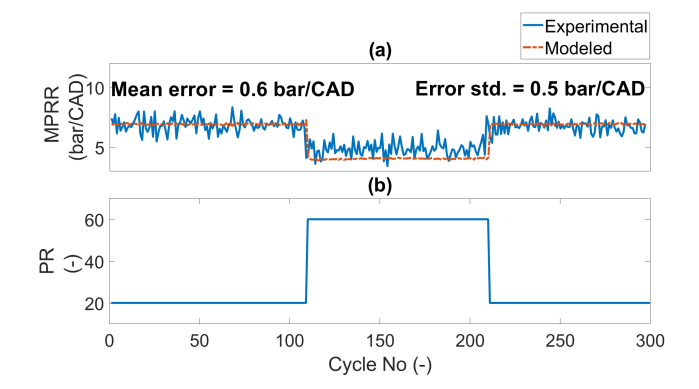


Fig. 1. Transient validation of the dynamic physics-based MPRR model [13]. Engine speed = 1000 RPM,  $T_{in}=60\,^{\circ}C$ , FQ = 22 mg/cycle, and SOI = 40 CAD bTDC.

# III. LINEAR PARAMETER-VARYING MODEL DEVELOPMENT

#### A. Data Driven Modeling (DDM)

An SVM based DDM is adapted in this work from Rizvi et al. [14] to develop state-space LPV representation for an RCCI engine. Eq. (1) and (2) present a discrete time LPV model:

$$x_{k+1} = A(p_k)x_k + B(p_k)u_k + K(p_k)e_k,$$
 (1)

$$y_k = C(p_k)x_k + e_k, (2)$$

where x, y and u are the states, measurable outputs, and the inputs to the plant, respectively. p represents the scheduling parameter, e represents stochastic white noise and k is the discrete time step. The matrices  $A(p_k), B(p_k), C(p_k)$  and  $K(p_k)$  are the state-space matrices of the plant as a function of the scheduling parameter p. The Eq. (1) and Eq. (2) can be rewritten as shown in Eq. (3) and (4):

$$x_{k+1} = \underbrace{(A(p_k) - K(p_k)C(p_k))}_{\tilde{A}(p_k)} x_k + B(p_k)u_k + K(p_k)y_k,$$
(3)

$$y_k = C(p_k)x_k + e_k. (4)$$

In this work, least-squared SVM (LS-SVM) is used to compute  $\tilde{A}(p_k), B(p_k)$  and  $C(p_k)$  matrices based on training data  $[x_k, u_k, p_k, y_k]_{k=1}^N$ . Matrices  $\tilde{A}(p_k), B(p_k), C(p_k)$  and

 $K(p_k)$  can be determined using Eq. (5) to (8):

$$\tilde{A}(p_k) = W_1 \Phi_1(p_k), \tag{5}$$

$$B(p_k) = W_2 \Phi_2(p_k), \tag{6}$$

$$K(p_k) = W_3 \Phi_3(p_k), \tag{7}$$

$$C(p_k) = W_4 \Phi_4(p_k), \tag{8}$$

where  $W_1, W_2, W_3$  and  $W_4$  are support vector weighting matrices and  $\Phi_1, \Phi_2, \Phi_3$  and  $\Phi_4$  are feature maps. All of these parameters are unknown and need to be determined. Eq. (3) and (4) can be rewritten as shown in Eq. (9) and (10):

$$x_{k+1} = W_1 \Phi_1(p_k) x_k + W_2 \Phi_2(p_k) u_k + W_3 \Phi_3(p_k) y_k,$$
 (9)

$$y_k = W_4 \Phi_4(p_k) x_k. \tag{10}$$

The least squares optimization method proposed by Suykens et. al [15] is used to compute the support vector weighing matrices using the cost function in Eq. (11):

$$J = \frac{1}{2} \sum_{i=1}^{3} ||W_i||_F^2 + \frac{1}{2} \sum_{k=1}^{N} E_k^T \Gamma E_k,$$
 (11)

where  $\Gamma$  is a diagonal matrix of the weighing factors for the estimation error known as the regularization matrix, and  $||.||_F$  is the Frobenius norm. The method of lagrange multipliers is used for minimizing the cost function shown in Eq. (11) as represented in Eq. (12):

$$\mathcal{L}(W_1, W_2, W_3, W_4, \alpha, \beta, e) =$$

$$J - \sum_{j=1}^{N} \alpha_j^T \{ W_1 \Phi_1(p_j) x_j + W_2 \Phi_2(p_j) u_j +$$

$$W_3 \Phi_3(p_j) y_j - x_{j+1} \} - \sum_{j=1}^{N} \beta_j^T \{ W_4 \Phi_4(p_j) x_j - x_{j+1} \}$$

$$= 2 \times 13$$
(12)

where j is discrete time and  $\alpha_j$  and  $\beta_j$  are the lagrange multipliers.

$$y_{k} = \underbrace{\sum_{j=1}^{N} \beta_{j} x_{j}^{T} \Phi_{4}^{T}(p_{j}) \Phi_{4}(p_{k}) x_{k} + \underbrace{\Gamma^{-1} \beta_{k}}_{e_{k}}. \quad (13)}_{W_{4}}$$

$$x_{k+1} = \underbrace{\sum_{j=1}^{N} \alpha_{j} x_{j}^{T} \Phi_{1}^{T}(p_{j}) \Phi_{1}(p_{k}) x_{k}}_{W_{1}}$$

$$+ \underbrace{\sum_{j=1}^{N} \alpha_{j} u_{j}^{T} \Phi_{2}^{T}(p_{j}) \Phi_{2}(p_{k}) u_{k}}_{W_{2}}, \quad (14)$$

$$+ \underbrace{\sum_{j=1}^{N} \alpha_{j} y_{j}^{T} \Phi_{3}^{T}(p_{j}) \Phi_{3}(p_{k}) y_{k}}_{W_{2}}$$

The global optimum of the lagrangian is found when the derivative is equal to zero, as it has a convex shape. The solution of the global optimum of lagrangian can be used to calculate  $W_1, W_2, W_3$  and  $W_4$ . Using that, Eq. (9) and (10) can be rewritten as shown in Eq. (13) and (14). The inner product  $\Phi_4^T(p_j)W_4\Phi_4(p_k)$  can be replaced with a kernel matrix as shown in Eq. (15) and (16):

$$[\Omega]_{j,k} = \sum_{i=1}^{3} z_i^T(j) \bar{k}^i(p_j, p_k) z_i(k), \tag{15}$$

$$[\Xi]_{j,k} = x_j^T \bar{k}^4(p_j, p_k) x_k,$$
 (16)

where  $z_1(k) = x_k$ ,  $z_2(k) = u_k$  and  $z_3(k) = y_k$ . In this work, a Gaussian kernel is used to perform kernel trick which is defined in Eq. (17):

$$\bar{k}^{i}(p_{j}, p_{k}) = exp(-\frac{||p_{j} - p_{k}||_{2}^{2}}{2\sigma_{i}^{2}}),$$
 (17)

where  $\sigma_i$  is the standard deviation for the Gaussian function and  $||.||_2$  is the  $l_2$  norm. Using the Eq. (15) and (16), state space form in Eq. (14) and (13) can be rewritten as Eq. (18) and (19):

$$X_{k+1} = \alpha \Omega, \tag{18}$$

$$Y = \beta \Xi + \Gamma^{-1} \beta, \tag{19}$$

where  $X_{k+1}$  and Y are the states and the outputs used in the training process. Thus,  $\alpha$  and  $\beta$  can be solved using the following equations:

$$\alpha = X_{k+1} \Omega^{-1},\tag{20}$$

$$vec(\beta) = (I_N \bigotimes \Gamma^{-1} + \Xi^T \bigotimes I_{n_y})^{-1} vec(Y),$$
 (21)

where  $\bigotimes$  represents the Kronecker product and vec(.) represents vectorization function.  $I_{n_y}$  and  $I_N$  are identity matrices. The classical Sylvester equation can be used to solve Eq. (21). Once  $\alpha$  and  $\beta$  have been computed,  $\tilde{A}(.), B(.), K(.)$  and C(.) are computed using the following equations:

$$\tilde{A}(\cdot) = W_1 \Phi_1(\cdot) = \sum_{k=1}^{N} \alpha_k x_k^T \bar{k}^1(p_k, \cdot),$$
 (22)

$$B(\cdot) = W_2 \Phi_2(\cdot) = \sum_{k=1}^{N} \alpha_k u_k^T \bar{k}^2(p_k, \cdot),$$
 (23)

$$K(\cdot) = W_3 \Phi_3(\cdot) = \sum_{k=1}^{N} \alpha_k y_k^T \bar{k}^3(p_k, \cdot),$$
 (24)

$$C(\cdot) = W_4 \Phi_4(\cdot) = \sum_{k=1}^{N} \beta_k x_k^T \bar{k}^3(p_k, \cdot),$$
 (25)

#### B. MPRR Model Identification

The RCCI dynamic model from Section II is used to generate data to train the SVM based identification model. The methodology explained in Section III-A is used to develop a state-space representation for RCCI combustion using data from the RCCI dynamic model. The data necessary for the

LPV identification has to be collected over the operating range of interest and should capture the dynamic behavior of the engine. The RCCI engine model is excited with a combination of inputs (Fuel Quantity (FQ), SOI and PR), and the output response (CA50,  $P_{soc}$ ,  $T_{soc}$ , IMEP and MPRR) of the model is recorded. The recorded output of the RCCI engine model is then used to identify the LPV representation.

The state-space representation for RCCI combustion is shown below in Eq. (26) to (29):

$$X = \begin{bmatrix} CA50 & MPRR & T_{soc} & P_{soc} & IMEP \end{bmatrix}^T, \quad (26)$$

$$U = \begin{bmatrix} SOI & FQ \end{bmatrix}^T, \tag{27}$$

$$p = [PR], (28)$$

$$Y = \begin{bmatrix} CA50 & MPRR & IMEP \end{bmatrix}^T. \tag{29}$$

The RCCI engine model is excited with inputs as shown in Fig. 2. The output response of the RCCI engine model is recorded as shown in Fig. 3. The combination of the input and output data generated from the RCCI engine model is used to train the data-driven SVM based LPV identification algorithm.

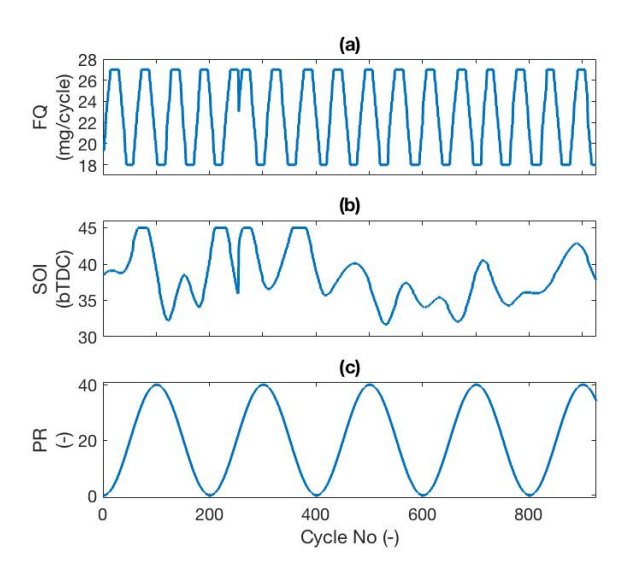


Fig. 2. Inputs to the RCCI dynamic model at N=1000 RPM,  $T_{in}=60$ 

Simulation data at a total of 926 operating points have been collected from the RCCI engine model. 65% of the data is used for training required in the SVM based LPV identification algorithm, while the remaining 35% of data is used for testing the identified state-space model. Fig. 4 presents validation of the identified LPV state-space models.

It can be observed that the SVM based state-space model can predict the MPRR with 0.4 bar/CAD mean error. The state-space matrix  $A(p_k)$  is plotted against the scheduling parameter, PR in Fig. 5. It can be seen that the relationship between the state-space matrices and the scheduling parameter is highly non-linear. This shows the advantage of using an LPV representation for the plant as it allows the state-space model to capture the plant's behavior accurately at

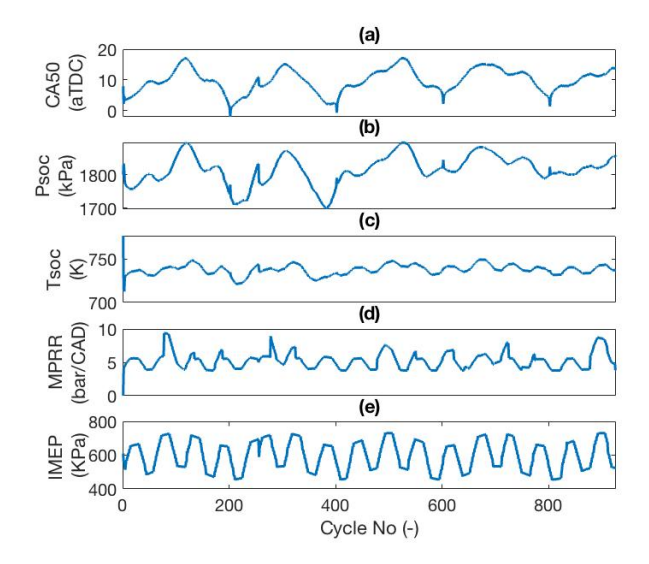


Fig. 3. State outputs from the RCCI dynamic model at N = 1000 RPM,

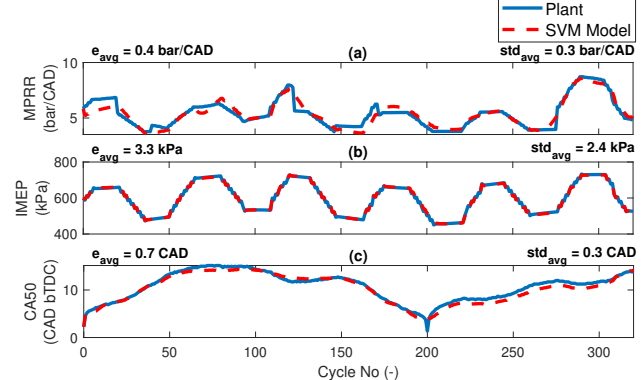


Fig. 4. Validation of data driven SVM based LPV identification at N = 1000 RPM,  $T_{in}$  = 60 °C every point of the scheduling parameter and not just a few points of linearization.

#### IV. DESIGN AND IMPLEMENTATION

#### A. Controller Design

An MPC framework is employed to adapt a linear time varying (LTV) representation of the RCCI engine using the state-space representation, as shown in Eq. (30) and Eq. (31):

$$X(k+1) = A(p(k)).X(k) + B(p(k)).U(k),$$
(30)

$$Y(k) = C(p(k)).X(k) + D(p(k)).U(k),$$
(31)

where k denotes the control time step and p(k) denotes the scheduling parameter as a function of the time step.

Fig. 6 depicts the schematic of the designed LPV-MPC controller. The SVM-based model learning approach generates LPV state-space representation of the plant based on PR as a scheduling parameter. Then, MPC uses the developed state-space representations to compute optimal control input. This state-space representation is updated and fed into the MPC at each time step which calculates the optimal control input. The controller solves a quadratic programming (QP) at each time step to optimize the manipulated variable adjustments. It solves the QP subject to the constraints defined

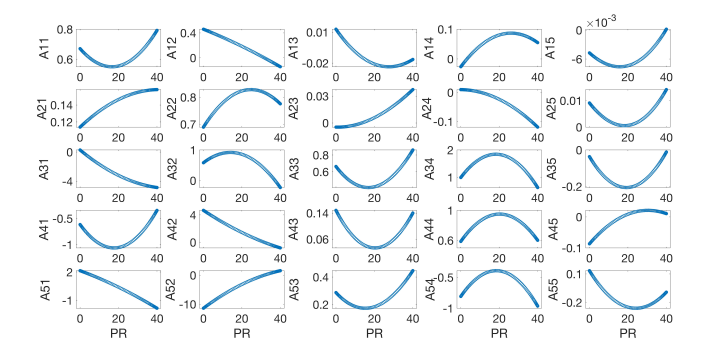


Fig. 5. Variation of  $A(p_k)$  matrix elements in the LPV setup as a function of the scheduling parameter (PR)

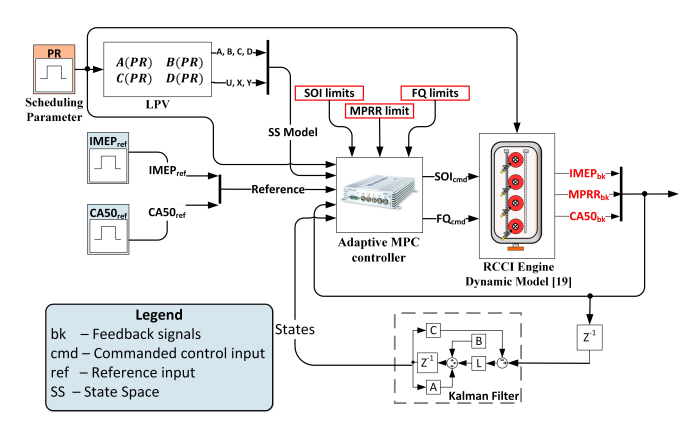


Fig. 6. Schematic of the designed LPV-MPC controller for the RCCI engine

on the inputs and the outputs. The optimization problem is only solved for the prediction horizon of 5 engine cycles. During each optimization, only a fixed number of control steps and control horizon are optimized. Invariably, the size of the control and prediction horizons affects the run time performance of the controller. The cost function used for the QP is shown in Eq. (32):

$$J(z_k) = J_y(z_k) + J_{\Delta u}(z_k) + J_{\epsilon}(z_k), \tag{32}$$

where  $J_y(z_k)$  is the cost function for reference tracking,  $J_{\Delta u}(z_k)$  is the cost function for manipulated variable rate of change and  $J_{\epsilon}(z_k)$  is the cost function for constraint violation. The cost functions are shown in the following equations:

$$J_y(z_k) = \sum_{j=1}^{n_y} \sum_{i=1}^p \left\{ \frac{W_{i,j}^y}{S_j^y} [r_j(k+i|k) - y_j(k+i|k)] \right\}^2$$
 (33)

$$J_{\Delta u}(z_k) = \sum_{j=1}^{n_u} \sum_{i=0}^{p-1} \left\{ \frac{W_{i,j}^{\Delta u}}{S_j^u} [u_j(k+i|k) - u_j(k+i-1|k)] \right\}^2$$

$$J_{\epsilon}(z_k) = \rho_{\epsilon} \epsilon_k^2 \tag{35}$$

Where  $z_k$  is the QP decision variable as shown in Eq. (36), p is the prediction horizon,  $n_y$  is the number of output states,  $n_u$  is the number of manipulated variables,  $y_j(k+i|k)$  is the predicted value of the  $j^{th}$  plant output at the  $i^{th}$  prediction horizon step,  $r_j(k+i|K)$  is the reference value for  $j^{th}$  plant output at the  $i^{th}$  prediction horizon step,  $S_j^y$  is the scale factor

for  $j^{th}$  plant output,  $W^y_{i,j}$  is the tuning weight of the  $j^{th}$  plant output at the  $i^{th}$  prediction horizon step,  $S^u_j$  is the scale factor for  $j^{th}$  manipulated variable,  $W^u_{i,j}$  is the tuning weight for  $j^{th}$  manipulated variable at the  $i^{th}$  prediction horizon step and  $\rho_\epsilon$  is the constraint violation penalty weight.

$$z_k^T = [u(k|k)^T \quad u(k+1|k)^T \quad ... u(k+p-1|k)^T \quad \epsilon_k]$$
 (36)

In Eq. (36)  $\epsilon_k$  is the slack variable at control interval k.

The MPC evaluates the specified constraints at every control step. The following constraints are imposed on the MPC:

$$\frac{y_{j,min}(i)}{S_{j}^{y}} - \epsilon_{k} V_{j,min}^{y}(i) \leq \frac{y_{j}(k+i|k)}{S_{j}^{y}} \leq \frac{y_{j,max}(i)}{S_{j}^{y}} + \frac{1}{S_{j}^{y}} + \frac{1}{S_{j}^{y}} + \frac{1}{S_{j}^{y}} + \frac{1}{S_{j}^{y}} + \frac{1}{S_{j}^{y}} - \epsilon_{k} V_{j,min}^{y}(i) \leq \frac{u_{j}(k+i-1|k)}{S_{j}^{y}} \leq \frac{u_{j,max}(i)}{S_{j}^{y}} + \frac{1}{S_{j}^{y}} + \frac{1}{S_{j}$$

$$\frac{\Delta u_{j,min}(i)}{S_{j}^{u}} - \epsilon_{k} V_{j,min}^{\Delta u}(i) \leq \frac{\Delta u_{j}(k+i-1|k)}{S_{j}^{u}}$$

$$\leq \frac{\Delta u_{j,max}(i)}{S_{j}^{u}} + \epsilon_{k} V_{j,max}^{\Delta u}(i), i = 1: p, j = 1: n_{u}$$
(39)

where,  $y_{j,min}(i)$  and  $y_{j,max}(i)$  are the bounds on outputs,  $u_{j,min}(i)$  and  $u_{j,max}(i)$  are the bounds on manipulated variables and  $\Delta u_{j,min}(i)$  and  $\Delta u_{j,max}(i)$  are the bounds on rate of change of manipulated variables.

#### B. Controller performance

The MPC is designed to track desired CA50 and IMEP while limiting the MPRR. An MPRR limit of 5.8 bar/CAD is selected as the constraint based on the experimental studies [5] on the same engine. A measurement noise based on experimental data [5] is also added into the CA50, IMEP and MPRR measurements to test the controller's performance. The results of tracking are shown in Fig. 7. The MPC is able to track the required CA50 and IMEP with mean error of 0.9 CAD and 4.7 kPa, respectively, while keeping MPRR below 5.8 bar/CAD.

However, we found out that increasing the reference IMEP above 6.5 bar results in degradation in tracking performance of the controller as shown in Fig. 8(a). Although the MPC is able to restrict the MPRR to 5.8 bar/CAD, the performance of CA50 is largely affected. This is because the main control variable for both MPRR and CA50 is SOI. Since, there is only one manipulated variable for two outputs, the performance of CA50 tracking, is degraded.

### V. CONCLUSIONS

A new control-oriented, data-driven state-space model was developed in this paper to predict MPRR in RCCI engines. The new model used an SVM method for representing RCCI dynamics in an LPV form. The new model was able to predict the CA50, IMEP, and MPRR with accuracy of 0.7 CAD, 3.3 kPa, and 0.4 bar/CAD, respectively. The LPV model

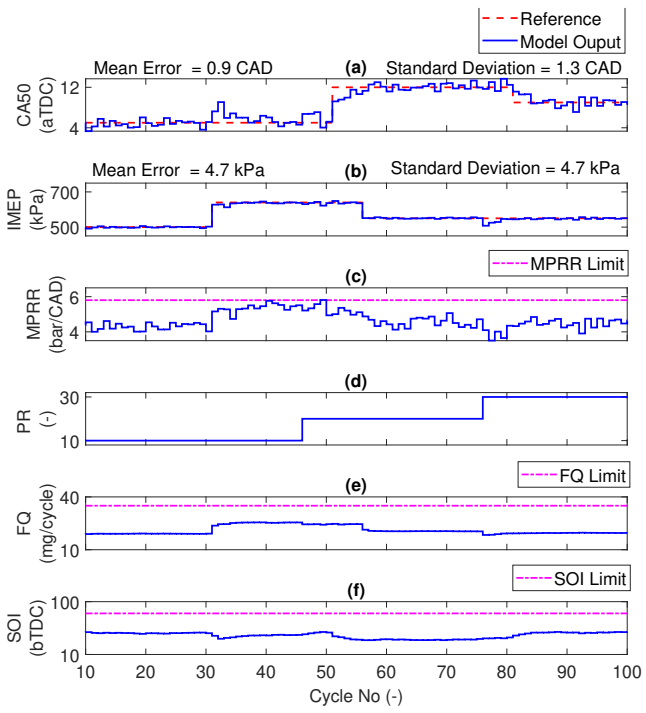


Fig. 7. CA50 and IMEP tracking with MPRR limitation

was integrated into an MPC framework to adjust MPRR, CA50 and IMEP for the RCCI engine. The new structure allows to cover broad engine load and PR conditions by smoothly transitioning among LPV model representations. The new RCCI controller is able to track the CA50 and IMEP with accuracy of 0.9 CAD and 4.7 kPa, respectively, while limiting the MPRR to 5.8 bar/CAD for engine loads below 6.5 bar. To cover broad engine load operation, another control input (e.g., DI fuel split) is required to enable simultaneous control of MPRR, CA50, and IMEP.

Our future work will include extending the current control framework by including more control inputs to allow independent control of CA50, IMEP while being able to independently adjust MPRR and  $\rm COV_{IMEP}$  within desired limits. In addition, the future work will include implementation of the designed control framework on our engine experimental setup.

#### ACKNOWLEDGMENT

This project is funded by the United States National Science Foundation under grants No. 1762520 and 1762595. The authors gratefully acknowledge Radhika Sitaraman and Sadaf Batool for their help in RCCI dynamic modelling and LPV-MPC design.

#### REFERENCES

- Ansari, E., Poorghasemi, K., Khoshbakht Irdmousa, B., and Shah-bakhti, M., "Efficiency and Emissions Mapping of a Light Duty Diesel
   Natural Gas Engine Operating in Conventional Diesel and RCCI Modes," SAE Technical Paper 2016-01-2309, 2016.
- [2] Zoldak, P., Sobiesiak, A., Bergin, M., and Wickman, D., "Computational Study of Reactivity Controlled Compression Ignition (RCCI) Combustion in a Heavy-Duty Diesel Engine Using Natural Gas," SAE Technical Paper 2014-01-1321, 2014.

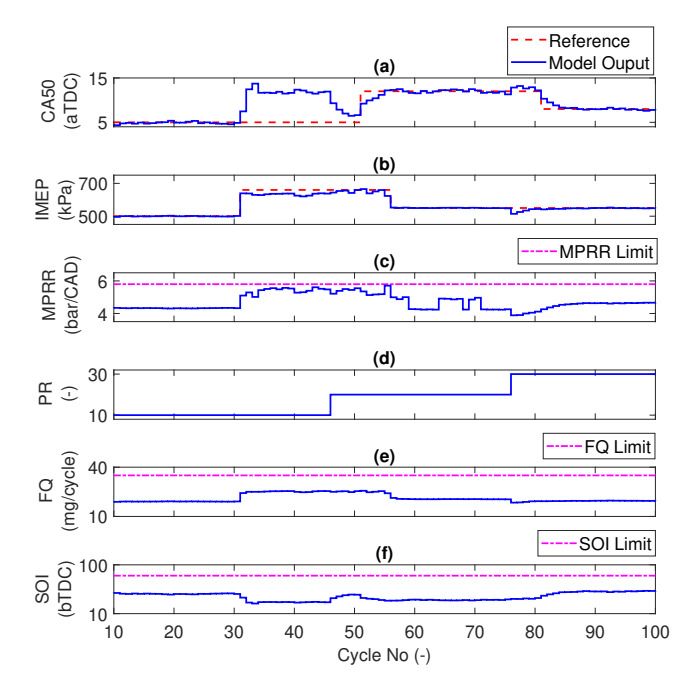


Fig. 8. Failed CA50 tracking with MPRR limitation, indicating the need for independent control inputs to adjust CA50 and IMEP

- [3] Sjöberg, M. and Dec, J., "Effects of Engine Speed, Fueling Rate, and Combustion Phasing on the Thermal Stratification Required to Limit HCCI Knocking Intensity," SAE Technical Paper 2005-01-2125, 2005.
- [4] Hanson, R., Curran, S., Wagner, R., and Reitz, R., "Effects of Biofuel Blends on RCCI Combustion in a Light-Duty, Multi-Cylinder Diesel Engine," SAE Int. J. Engines 6(1):488-503, 2013.
- [5] Kannan, K., "An Experimental Investigation Of Low Temperature Combustion Regimes In A Light Duty Engine", Open Access Master's Thesis, Michigan Technological University, 2016.
- [6] Arora, J. and Shahbakhti, M., "Real-Time Closed-Loop Control of a Light-Duty RCCI Engine During Transient Operations," SAE Technical Paper 2017-01-0767, 2017.
- [7] Kondipati, N.N., Arora, J.K., Bidarvatan, M., and Shahbakhti, M. (2017). "Modeling, design and implementation of a closed-loop combustion controller for an RCCI engine," 2017 American Control Conference (ACC), 4747-4752.
- [8] Sadabadi, K.K., and Shahbakhti, M., "Dynamic Modelling and Controller Design of Combustion Phasing for an RCCI Engine." Proceedings of the ASME 2016 Dynamic Systems and Control Conference, Volume 2.October 12–14, 2016. V002T20A004.
- [9] Shahbakhti, M., Ghafuri, M., Aslani, A. R., Sahraeian, A., Jazayeri, S. A., and Azadi, S. (April 26, 2010). "A Method to Determine Fuel Transport Dynamics Model Parameters in Port Fuel Injected Gasoline Engines During Cold Start and Warm-Up Conditions." ASME. J. Eng. Gas Turbines Power. July 2010; 132(7): 074504.
- [10] Raut, A., Irdmousa, B. and Shahbakhti, M., "Dynamic Modeling and Model Predictive Control of an RCCI Engine", Control Engineering Practice, Vol. 81, Pages 129-144, 2018.
- [11] Indrajuana, A., Bekdemir, C., Luo, X., and Willems, F. (2016). "Robust multivariable feedback control of natural gas-diesel RCCI combustion." IFAC-PapersOnLine, 49(11), 217-222.
- [12] B. K. Irdmousa, S. Z. Rizvi, J. M. Veini, J. D. Nabert and M. Shahbakhti, "Data-driven Modeling and Predictive Control of Combustion Phasing for RCCI Engines," 2019 American Control Conference (ACC),pp. 1617-1622.
- [13] Basina, A., "Modeling and Control of Maximum Pressure Rise Rate in RCCI Engines", Open Access Master's Thesis, Michigan Technological University, 2019.
- [14] Rizvi, S. Z., Mohammadpour, J., Tóth, R., and Meskin, N. (2015). "A kernel-based approach to MIMO LPV state-space identification and application to a nonlinear process system." IFAC-PapersOnLine, 48(26), 85-90.
- [15] Suykens, J. A., and Vandewalle, J. (1999). "Least squares support vector machine classifiers." Neural processing letters, 9(3), 293-300.